DOI: 10.37190/abb/208611

Automated biopsy path planning and navigation using a novel software-hardware platform

Adam Ciszkiewicz[1], Jakub Urban[2], Grzegorz Ziółkowski[2], Celina Pezowicz[2], Ewelina Świątek-Najwer[2*]

[1]Faculty of Mechanical Engineering, Cracow University of Technology, Cracow, Poland

[2]Faculty of Mechanical Engineering, Wrocław University of Science and Technology, Wroclaw, Poland

[*]Corresponding author: Ewelina Świątek-Najwer, Faculty of Mechanical Engineering, Wrocław University of Science and Technology, e-mail address: ewelina.swiatek-najwer@pwr.edu.pl

Submitted: 30th May 2025

Accepted: 24th July 2025

Abstract:

Purpose: Image-guided biopsy is essential for safe and precise procedures, our main aim was to develop a software-hardware platform for assisting and automating this task. Methods: This study presents a prototype hardware-software platform for biopsy assistance, featuring an optimization tool for preplanning and the MentorEye system for real-time needle navigation using a simple support setup. Evaluation was conducted on a custom skull phantom with brain tissue and cancerous lesions. The system optimizes needle paths while considering surrounding structures and provides intraoperative guidance. Results: The planning tool successfully generated viable trajectories for all lesions, typically aligning with the shortest insertion paths. The mean Target Registration Error between CT and optical navigation was 2.08 ± 0.43 mm. In seven simulations, all biopsies were successful, with a mean deviation of 2.15 ± 0.84 mm and an nRMSE of 3.7%. Conclusions: The accuracy of the surgery simulation was influenced by segmentation, registration procedure, possible brain shift between imaging and intraoperative position, navigation system errors, and manual errors by the operator. Experiment results confirmed good efficiency of developed tools for automatic planning and image-guided aiding biopsy.

Keywords: Differential evolution; Largest Empty Sphere; Lesion; Needle; computer assisted biopsy; tracking system

1. Introduction

Recent literature reviews suggest a large number of studies in semi-autonomous and autonomous surgical procedures [20]. Automating medical procedures is a key aspect in the advent of medical staff shortages [40]. Biopsy is one of the key procedures in medical science, its purpose lies in reaching pathological targets within the body, while avoiding healthy tissues. The samples obtained this way can be used for diagnosis and treatment planning in many areas of medicine, such as oncology.

Automatic path planning for biopsy is an important part of autonomous medical treatment systems. In this area, the path for the needle is computed automatically by an algorithm using medical scans with limited or no input from the clinician. The main advantage of automatic planning is increased efficiency of biopsy, which results in reduced complications risk. These methods are also a major support for inexperienced physicians and might serve as training systems. Nevertheless, the planned paths need to be minimally invasive and planning such paths requires specialized approaches. The problem of path planning is well known in robotics and currently many methods are available, with examples including graph-based approaches [21], through popular tree-based solutions often using

triangular meshes [25], and into optimization [1, 5]. Employing these various techniques is also very common in biopsy planning [30] with various custom approaches presented, examples including: prospective stereotaxis combined with skull-mounted trajectory guides and rapid trajectory design [12], path planning for Baker's cyst biopsy based on differential evolution [6], path generation with Lagrange multipliers and 3d vectors [32], 3D ultrasound-guided system visualizing needle paths in real-time with planning optimal routes while avoiding blood vessels and ribs [2] and path planning [14] within a combined automated biopsy system, with comparisons to manual planning available in [17], as well as multiple specific applications for neurosurgery as noted in [19] and [36], including [3, 22, 34]. Nevertheless, with the complex and uncertain nature of path planning in biological structures the issue still remains open. These automated solutions are typically based either on a cost map, which is a modified representation of the medical scan or actual distances from critical structures. Regardless of the approach, these methods provide tools to numerically assess the paths and subsequently select the best one using some optimization or brute-force search.

Automatic path planning has specific advantages with researchers reporting perpendicular entry, shorter trajectory lengths and lower risk compared to manual planning [17]. Computer aided biopsy also enables significantly shorter operative times, reduced blood loss, and improved patient outcomes compared to traditional surgical techniques, reducing the risk of postoperative complications. However, challenges still remain, such as compensating for respiratory movement in certain procedures. There are also not enough outcomes regarding practical application of automatic planning in clinical conditions [30], since the physician must be aware of anatomical variability, possible patient movements and necessary adaptation while procedure.

Computer assisted biopsy procedures may also leverage the use of robotic arms to increase accuracy of needle placement precision according to designed scenarios on integrated imaging techniques (CT, ultrasound, MRI) [4, 24, 15]. The robotic arm reduces time of surgery, as the surgeon does not need to manipulate to reach the proposed position and trajectory line and help to reduce the radiation dose for the surgical team [4, 15]. These robotic image-guided systems often cooperate with optical tracking devices. The system described in the study of Treepong [33] provided a higher success rate of breast biopsy (equaled 80%). An important feature of robotic image-guided systems, present even in the early systems, is the ability to adjust the trajectory knowing the current 3d error [27].

This error varies in biopsy depending on anatomical region, imaging modality, and system used, and can range from 2.1 mm to over 10 mm [7, 9, 11, 15, 24, 26, 29, 39].

Ultrasound and MRI-guided systems differ significantly in accuracy, and augmented reality has been proposed to improve ergonomics and planning. Despite its potential, AR still requires high-resolution, low-latency systems and precise calibration to match virtual data with the user's spectroscopic perception [16].

While many solutions for automated biopsy are available, due to the uncertain and complex nature of the problem, the issue still remains open. Therefore, the aim of this study is to propose and validate a platform for automatic biopsy based on a hardware needle tracking system and computer software for path optimization. This study is based on and significantly extends previous works [16, 23] and [6]. In [16, 23] a hardware system named MentorEye was proposed. It is a complex computer assisted surgical system for planning and aiding biopsy, resection and reconstruction surgery mainly in the craniofacial area. The MentorEye system applies CT DICOM dataset and the user identifies the tumor and design tumor biopsy or resection with proper safety margins. In reconstructive surgery planning the tool also helps to design geometry of bioimplant to reconstruct post-resection bone loss. Subsequently the system can be applied intraoperatively in order to control the resection and reconstruction surgery under control of optical (Polaris Spectra) or electromagnetic (Aurora) tracking systems from Northern Digital Inc., Canada. The software provides point-pair and novel hybrid registration techniques [31]. MentorEye enables an ergonomic visualization with augmented reality goggles [16, 23] or typical external monitor visualization, applied in this study. In terms of the planning solution study [6] presents a cost-map based approach for Baker's cyst. The approach defines the path planning through an objective function and solves the problem with metaheuristic optimization. The needle path is planned in two dimensions within the assumed insertion plane. The software is capable of providing viable needle insertion paths with customizability through its various parameters.

In the current study, our main aim was to combine and extend both the hardware and the software part into one system and perform its initial verification using a 3D printed phantom. In order to do so, the MentorEye system was adapted to use a high resolution CT dataset for planning and aiding biopsy surgery. The planning procedure from [6] was significantly extended to a three-dimensional dataset and fitting a 3D sphere to the identified shape of identified lesion, which also resulted in a more complex optimization procedure capable of returning realistic needle insertion paths. The results showcased the viability of the system through successful execution of planned paths on the skull-brain phantom with 7 lesions.

2. Materials and Methods

This study presents a comprehensive hardware-software solution for simulating biopsy procedures. An example application presented in this article is brain biopsy. However, the developed tool is not limited to this domain. The “Materials and Methods” section was subdivided into two parts. First one focused on the proposed software for biopsy preplanning, while the second one described the hardware used to execute navigated biopsy based on the preplanned paths for the needle. The software subsection covered two main issues: image preprocessing, to obtain the collision map and targets, and path planning using the obtained map. The hardware subsection focused on calibrating the computer aided intraoperative system (calibration of surgical tools and registration procedure), performing biopsy using a simple support system under control of optical tracking system and with visualization on CT scan and description of analyzed quantitative results of simulations.

2.1. Object of study

As mentioned before, the system aids biopsy procedures. Therefore, in order to test it in realistic conditions a skull and brain phantom was 3D-printed. The skull phantom (see Figure 1) contained 3D printed brain tissue and multiple simulated lesions. The brain part was created from synthetic material, and the lesions were filled with plasticine. Lesions were inserted only in selected target planes to simplify the procedure and ensure that the phantom did not break. The phantom was scanned using a Waygate V|tome|x M300/180 scanner at a voltage of 250 kV and a tube current of 200 mA, resulting in 1398 layers of imaging data with specific parameters: pixel spacing of 0.1305 mm, a slice thickness of 0.13 mm, and a field of view of 234.93 mm.

At this stage, the verification of the system was performed in simplified conditions to ascertain whether the automatically planned biopsy target and path can be fulfilled under control of the tracking system after the registration procedure. The main focus was on the navigation accuracy and the possibility to actually execute the planned path with relation to the phantom. Possible material deformations caused by needle insertion were not investigated in this study. Therefore the approach to the lesions was opened, as seen in Figure 1c. While this simplified the procedure, it did take into account all other possible factors - discrepancies between the real position of the brain object inside the skull and location recorded on CT, segmentation errors while planning, inaccuracy of registration procedure, navigation system error and operator’s manual error.

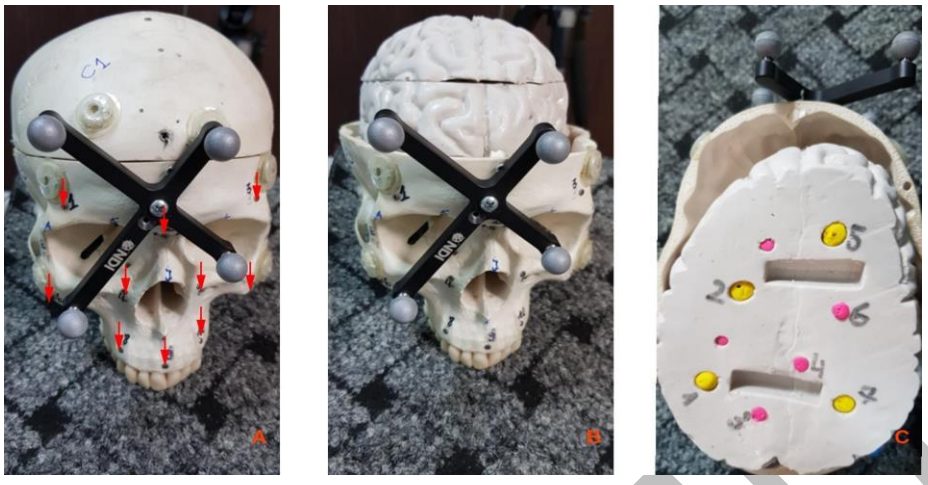

Figure 1. *Skull and brain phantom with 7 tumor lesions in three different configurations: A – skull phantom, arrows indicate fiducials, B – brain, C – target plane with tumor lesions.*

2.2.1. Preprocessing medical image data.

Preplanning needle biopsy is a complex problem, which revolves around computing the starting and target points for the needle so that the resulting path is minimally-invasive and safe. In this study it was addressed in a unique way, tailored to take advantage of native representations of medical image data, that is three-dimensional voxel arrays. The custom planning procedure was written in Python.

2.2.2. Thresholding the voxel array to select the target point for biopsy.

The procedure required a 3D DICOM dataset as an input and a target object for biopsy, without specifying the actual target point. This DICOM dataset was converted into a 3D integer array using PyDICOM [18]. Then, multilevel thresholding was performed. Its levels were selected manually to represent the bone, the gray matter and the target objects representing malicious tissue. These thresholded binary images were saved into separate 3D voxel arrays: binary_bone, binary_graymatter, binary_targets. In the next step, the binary_targets array underwent conditional labeling based on object volume using scikit-image [37]. This resulted in a list of viable target objects within the image. Then, the actual biopsy target, selected by the user, was saved into its separate voxel array binary_target and removed from the original binary_targets array.

2.2.3. Computing the cost map.

In order to obtain the path, a representation of the collisive space was needed. The proposed method employed a grid based on the original CT image, which contained the cost of traveling through the voxel, which is frequently used in robotics. In order to do so, every tissue was assigned a weight, representing its importance. In this study, the highest weight was assigned to the lesions, as the brain phantom had multiple elements of that kind. With the

weights set, the voxel values corresponding to the specific tissues were replaced with the weights, similarly to Trope [34] and Ciszkiewicz [6] to create an initial cost map costmap_ini by a weighted sum on the obtained binary images:

(1) $costmap\_ini[x,y,z] = w_{gm} * \text{binary\_graymatter}[x,y,z] + w_b * \text{binary\_bone}[x,y,z] + w_t * binary\_targets[x,y,z]$

where w_gm, w_b, and w_t were the weights assigned to grey matter, bone, and targets, respectively. Note that the cost map did not contain the actual target lesion. Its cost was reflected in the final objective function explained in the following sections. In the next step, the map was smoothed, to create additional safety regions around the most important tissues and augmented with additional constraints on the surgical space using voxelized spheres with position and radius selected by the user:

(2) $costmap\_fin[x,y,z] = costmap\_ini[x,y,z] + s * (\text{gaussian\_filter}(\text{costmap\_ini}[x,y,z], \sigma)) + \sum(w_{si} * voxelize\_sphere(center, radius))$

where: s – the scaling factor, σ - standard deviation for Gaussian kernel, voxelize_sphere – a function, which returned a 3D binary image of the same shape as costmap_fin containing a voxelized sphere with a specified center and radius, ones in the image represent points within the sphere, while zeroes reflect the background, w_si – the weights assigned to the spheres, representing the cost of traveling through the sphere.

In this study, two additional spheres were used. The first one was inserted in the front of the face, covering the eyes, mouth, and the frontal part of the brain. It was meant to discourage the procedure from finding dangerous and unconventional paths for needle insertion. The second sphere was inserted on the bottom of the image and covered the neck and the lower parts of the brain to limit the access to the lower part of the brain, increasing the safety of the procedure.

2.2.4. Estimating the target point

In this study, the target point estimate for the biopsy was the center of the Largest Empty Sphere (LES), which can be fitted inside the target object. Although there are many ways to obtain the LES, this study takes advantage of the Exact Euclidean distance transform as implemented in Scipy [38].

2.2.5. Path planning

The computed cost map and the estimate of the target point form the input to the actual path planning procedure, which is formulated as an optimization problem. The main objective of path planning was to find a needle path, starting outside of the skull and ending close to the estimate of the target point with the lowest possible travel cost based on the costmap.

The needle was assumed to be rigid. Therefore, its path was fully defined by its starting point and target point. The needle radius was assumed to be much higher than that of the typical surgical needle to account for uncertainty when the actual path executed. Given these points and the needle radius, the needle was voxelized into an array of the same shape as the costmap. The cost of the path was then simply a sum of the product of the two arrays:

$$(3)\text{path\_cost} = \sum\left(\text{costmap\_fin}[x, y, z] * \text{voxelize\_needle}(\text{starting\_point}, target\_point, radius\_needle)\right)$$

where: path_cost – the numerical cost of the needle traveling through the path given by its starting_points and target_point under the assumed radius of the needle radius_needle, voxelize_needle – a function, which returned a 3D binary image of the same shape as costmap_fin containing a voxelized needle with the specified starting_point, target_point and radius_needle, ones in the image represent points within the needle's representation, while zeroes reflect the background.

2.2.7. Objective function

The path_cost defined in the previous subsection formed the basis of the objective function, which was used to rate the needle paths within the optimization procedure. The final objective was a weighted sum of two subobjectives: the aforementioned path_cost and the distance from the actual target point to its estimate given by the center of the LES:

$$(4) f(x) = w1 * path\_cost + w2 * dist\_to\_LES\_center,$$

where: f(x) - the objective function used to rate the path with x being the decision variable vector specifying the path, w1 and w2 - the weights signifying the importance of each subobjective, dist_to_LES_center - the second subobjective, which featured nonlinear distance scaling heavily favouring the target points in the closest vicinity of the LES center, while heavily penalizing solutions outside of the LES, akin to Ciszkiewicz [6].

The vector of the decision variables x contained 5 variables in this case. This included, two angles θ and γ to represent the spatial orientation of the needle in the spherical coordinate system and three coordinates of the actual target point target_point:

$$(5) x = [\theta, \gamma, x_{target}, y_{target}, z_{target}]^T$$

where: θ, γ - the angles defining the orientation of the needle, x_target, y_target, z_target - the coordinates of the target point vector target_point. The angles were allowed to change in their full ranges, as the actual surgical space was constrained by the additional spheres, the target coordinates were limited to the bounding box of the target object from the binary_target image.

2.2.8. Optimization algorithm

In this study, the algorithm used to minimize the objective function f(x) and find the optimal, minimally-invasive needle path was a hybrid between Differential Evolution (DE) and Nedler-Mead (NM) approach [10]. DE is a modern representative of a large group of metaheuristic optimization algorithms known for their global convergence, while NM is a popular choice in refining solutions of global optimizers. When combined, they provide an efficient way to estimate the global minimum of the objective function. Both algorithms were sourced from a Python library Scipy [38], with the DE parameters set to maxiter = 100 and popsize = 25 and the rest remaining default for both DE and NM.

2.3. Hardware navigation

In the second part of the study, the optimized needle paths along with the imaging data were imported into the MentorEye system for image-guided assistance. The MentorEye system provided computer-aided navigation using the Polaris Spectra infrared optical navigation system from Northern Digital Inc. MentorEye was a system developed to support biopsy procedures within a software-hardware platform (Figure 2) [16, 23]. The software did not feature automatic path planning for the needle but enabled needle tracking in real-time based on the user-provided start and target points enabling manual biopsy planning.

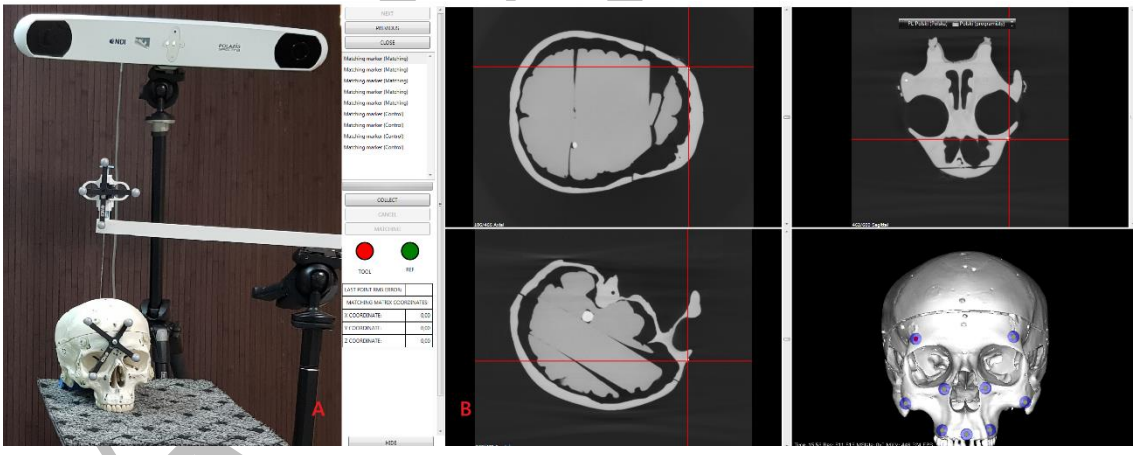

Figure 2. *MentorEye system with biopsy support stand (A). Localization of titanium fiducials applied for registration procedure and control points (B).*

Within this study, the planning part of the system was extended to enable importing the automatically planned needle paths from the procedure described in the previous chapters. The resulting system guided the physician through the particular stages of intraoperative support according to automatically obtained needle paths. The user could observe real-time position of needle related to the three CT projections and in 3D view of skull phantom and the obtained start and target points. Additionally, there were three indicators presenting the deviations in x, y, and z coordinate and one indicator presenting the angle deviation of

trajectory. In order to employ the system within the phantom experiment several steps were required. These included: calibration of tracked tools (pointer, biopsy needle), point-pair registration procedure and finally image-guided biopsy, described in detail in the subchapters.

2.3.1. Navigation System Calibration

Firstly, calibration files for instruments used during the simulation were selected, and a frame of reference was affixed to the phantom possibly close to the operation field. A pointer was pivoted to determine its actual tip offset. The biopsy needle was calibrated in order to obtain the coordinate system with an origin located on the needle tip and with a coordinate axis parallel to the long axis of the needle. Therefore the visualization of needle real-time direction is self-explaining.

A point-pair registration procedure was executed utilizing titanium markers implanted in the phantom, with five matching points used to derive the registration matrix. Localization of fiducials - titanium markers is presented in Figure 1 and Figure 2. In order to achieve the registration matrix the corresponding pair of points were marked on the CT dataset and with a tracked pointer. The point-pair registration algorithm solved the registration matrix. Fiducial Registration Errors (for fiducials applied in calculations) and Target Registration Errors (for control points) were calculated. If the errors exceed 3 mm the procedure was repeated.

2.3.2. Biopsy Procedure

The biopsy simulation involved a simple support system designed to guide the biopsy needle along an optimized trajectory. The setup was built using an adjustable photo stand integrated with a square-profile beam, which was drilled on the opposite side (Figure 2). A 20G x 130 mm needle was inserted through two selected holes in the profile. The biopsy procedure was performed with the skull cap and the upper slice of the phantom brain removed to eliminate the influence of simulated brain tissue stiffness.

2.3.3. Assessing the results from the experiment

In order to assess the quality of the obtained results, the following metrics were used:

- **visual assessment** of whether the needle punctured the selected lesion during biopsy,
- **Fiducial Registration Error (FRE)**: is the distance error for the fiducial i as seen in CT and after the registration

(8) $$FRE_i = \| \mathbf{T}\,(\mathbf{p}_{NAV,i}) - \mathbf{p}_{CT,i} \|$$

where:

T - the registration matrix and the corresponding points,

$\mathbf{p}_{CT,\,i}$,- homogeneous coordinate vector of the fiducial point *i* (where $I \in <1, 5>$) in CT,

$\mathbf{p}_{NAV,\ i}$ - homogeneous coordinate vector of the corresponding fiducial *i* point measured by navigation were used to calculate **T**,

- **Target Registration Error (TRE)**: is the distance error of the target fiducial markers after the registration,

  (9) $$TRE_i = \|\mathbf{T}\ (\mathbf{p}_{NAV,\ i}) - \mathbf{p}_{CT,\ i}\|$$

  where:

  T - the registration matrix and the points

  $\mathbf{p}_{CT}$,- homogeneous coordinate vector of the fiducial point *i* (where $i \in <6, 9>$) in CT,

  $\mathbf{p}_{NAV}$ - homogeneous coordinate vector of the corresponding fiducial *i* point measured by navigation, were **not** used to calculate **T**,

- **linear and angular deviations** between planned and performed trajectory of biopsy and nRMSE (normalized Root Mean Square Error) on the distance from the planned target point to the actual target point; normalized by the average length of the path.

3. Results

3.1. Path planning in Python

The proposed automatic system for biopsy planning identified 14 lesions of suitable size through thresholding and object labeling. The targets were of irregular shape, which was reflected in the ratio of LES area to the target area averaging at 49.0 ± 8.2 % with radii of 3.1 ± 0.7 mm. The planning procedure optimized needle paths for all of them. These paths were presented in Figure 3. All of the obtained target points were within their corresponding LES. Most of the paths were mostly perpendicular to the skull surface, which highlighted the effectiveness of the procedure at finding the short, safe paths.

3.2. Registration Accuracy

Out of the 14 planned paths, 7 that were possible to reach within the prepared skull phantom were selected for further testing in real-world space.

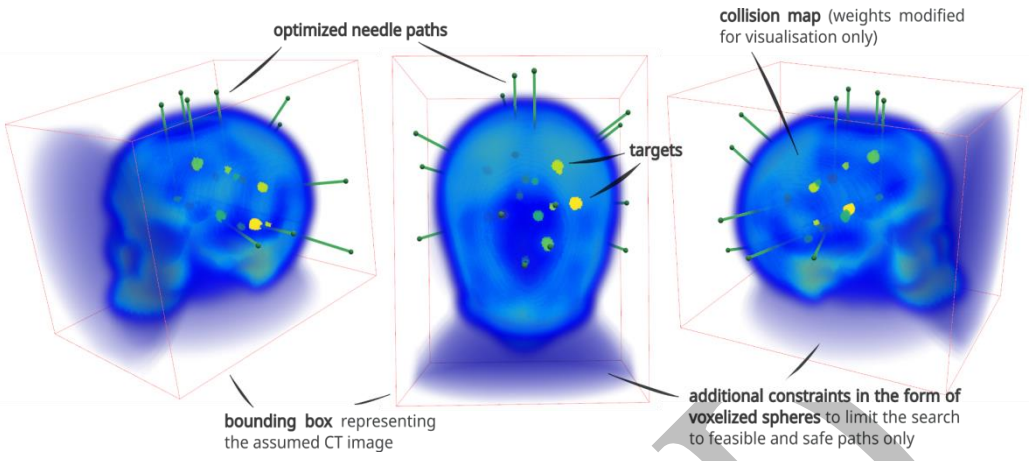

Figure 3. *The needle paths obtained from the proposed path planning procedure as seen from three different perspectives and drawn on top of the collision map and the lesions/targets. Red and blue colors signify high and low cost of traveling through voxels respectively.*

3.3. Biopsy results

The biopsy was performed on all of the seven selected lesions. Each stage of the procedure, including the contact point setup and the actual insertion of the biopsy needle, was closely monitored via the MentorEye system (Figure 4A). A visual inspection of the lesion for needle punctures was performed after biopsies. In seven out of seven lesions, the lesion was properly punctured allowing for safe biopsy, see Figure 4B. Table 2 contained summarized deviations between planned and achieved target positions and trajectories and result of visual inspection of the lesion (hit or not). In all cases the lesion was properly hit. The mean distance between target point and planned position equaled 2.15 ± 0.84 mm.

3.3. Biopsy results

The biopsy was performed on all of the seven selected lesions. Each stage of the procedure, including the contact point setup and the actual insertion of the biopsy needle, was closely monitored via the MentorEye system (Figure 4A). A visual inspection of the lesion for needle punctures was performed after biopsies. In seven out of seven lesions, the lesion was properly punctured allowing for safe biopsy, see Figure 4B. Table 1 contained summarized deviations between planned and achieved target positions and trajectories and result of visual inspection of the lesion (hit or not). In all cases the lesion was properly hit. The mean distance between target point and planned position equaled 2.15 ± 0.84 mm.

In the first step, the accuracy of the navigation system was assessed with error metrics: FRE and TRE calculated for the markers. Their peak values were at 1.64 mm and 2.66 mm for FRE and TRE respectively with mean of only 1.01 ± 0.59 mm and 2.08 ± 0.43 mm.

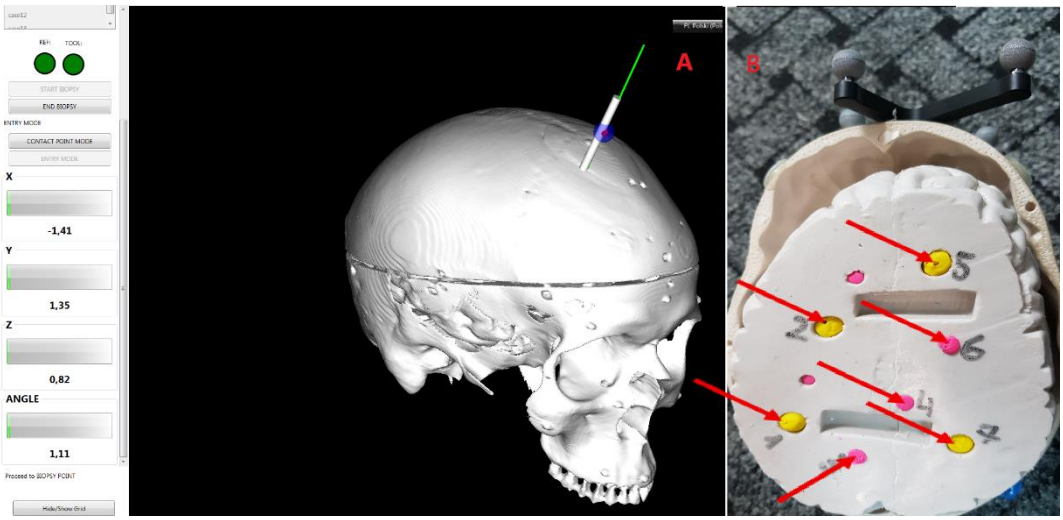

Figure 4. A sample biopsy procedure in MentorEye system for target #5 as seen in Figure 1 (A). Result of biopsy procedures (arrows indicate punctures in plasticine lesions) (B).

Table 1. Visual inspection result, deviations between planned and achieved positions and trajectories for seven lesions, where: insp. - the result of the visual inspection of the incision, which could be either: hole - a small incision recognized after biopsy, trace - a larger incision was observed after the biopsy, when the planned trajectory angle relative to the tangent plane was close to zero, xdiff, ydiff, zdiff - deviation in x, y, z coordinates of target point regarded planned position, d - distance between target point and planned position, α - angle between achieved and planned trajectory.

Id	insp.	x_{diff} [mm]	y_{diff} [mm]	z_{diff} [mm]	d [mm]	α [deg]
1	+ (trace)	-1.76	-1.26	-2.29	3.15	1.56
2	+ (hole)	0.2	-0.19	2.19	2.21	2.68
3	+ (hole)	0.61	-1.03	-0.4	1.26	0.31
4	+ (hole)	-0.87	-0.5	0.91	1.35	1.68
5	+ (hole)	-1.41	1.35	0.82	2.12	1.11
6	+ (hole)	0.46	-0.48	1.43	1.58	1.17
7	+ (trace)	-0.58	-1.36	-3.03	3.37	1.67
		Mean ± Standard Deviation			2.15 ± 0.84	1.45 ± 0.72

Figure 4B illustrated the incisions resulting from the biopsy procedures, providing a visual representation of the needle penetrations in the simulated lesions. Based on the

obtained results the nRMSE calculated using the distance from the planned target point to the actual target point and normalized by the average length of the path equaled 3.7%.

4. Discussion

4.1. Software path planning

As mentioned before, this study was based on imposing a voxelized needle representation onto a cost-map for the needle path planning. The approach was successful in providing minimally-invasive and safe paths under the assumed conditions for the assumed phantom of the skull and brain. This voxelized-needle approach is in contrast with some of the other studies in medical path planning [17] and [28], where the risk is assessed as the sum of the distances from vessels, or potentially other dangerous elements. While cost-maps or distance maps have been used for path planning, as seen in [3], the use of a voxelized cylindrical needle allowed for indirect inclusion of uncertainty. This uncertainty is reflected in the radius of the needle within the obtained path. While this approach is more numerically expensive than tracing a single path line, as seen in [3], it is also more robust to uncertainty.

Our other contribution in this area is in employing Largest Empty Spheres for target point estimation, which then further optimized. The center of the LES in an object represents a point, for which the minimal distance to the object boundary is the highest amongst all of the points within the object. From a geometric point of view, it represents a point with the highest margin of error when executing a biopsy. This is in contrast to some of the available studies. In [17] and [28] this problem was addressed by using a risk minimization procedure, which transforms the target object into a structure similar to a cost-map or other approaches featuring voxel-based search for entry points [3]. All of these approaches are viable, as shown in their respective studies. Nevertheless, they also partially determine the procedure for the path planning. In the current study, the use of the LES allows for transforming the discrete search space defined by the voxels into a continuous one defined by the target point and the entry point, all while making no assumptions on the underlying CT data, which is only segmented with no need for the creation of specific meshes or other elements. This means that the search for the optimal path can be then executed by an optimization procedure in the continuous space, without tying the results to the resolution of the voxel image or the obtained meshes, which might be the case with other approaches [17] and [28]. Additionally, having the target to be inside the LES makes it possible to generalize the path more - in this case the path is specified by five variables, out of which two define the orientation of the needle and three are the actual target coordinates. This potentially allows for safer paths, as the software

can work with more degrees of freedom - 5 - in contrast to 3 in some of the available studies [35] or number of presampled entry points [13, 22, 34] or vertices of a mesh [17, 28].

4.2. The effectiveness of the hardware part and the entire system

During testing, deviations in trajectory (angle) and target position (x, y, z coordinates and distance) were measured. However, the most important metric in the entire experimental setup was the visual inspection of the targets. In these terms, the proposed system had very good performance with needle reaching seven out of seven targets. This meant that the navigational part of the system was working as intended. The mean accuracy in our tests: 2.15 ± 0.84 mm was comparable to a previous study with CT guided biopsy [16] and CT and AR-guided osteotomy [23]. Regarding the mean angular deviations of 1.45 ± 0.72 degrees were much better than in [23]. The nRMSE of 3.7% target displacement is also a satisfactory result. Obtained results were comparable to those reported for robotic-assisted systems [7, 9, 24, 26, 29, 39]. Probable reason for that was a high resolution of scan and applied titanium markers. The main source of error in the proposed approach was manual human error resulting from free-hand operation with a stand. Minimizing it would lower the inaccuracy of biopsy even more, which is important if we consider tissue stiffness instead of air traverse to lesion.

As mentioned before, the study was carried out using a 3D printed skull-brain phantom. The use of phantoms was common in other related studies, such as [14] and [8]. This phantom served as the baseline for obtaining the CT used for path planning. It was also used during the experimental part to test the obtained paths with proper navigational support. It should be mentioned that the experimental part was carried out in simplified conditions with the skull opened and the target plane revealed. At this stage, the aim of the experiment was to assess the effectiveness of the system at navigating the surgeon to the very small target objects inside the brain, reflected by the small radii of all of the obtained LES.

4.3. Limitations

Although the system was proven effective in undertaken tests, some limitations should be acknowledged. Regarding the software, the needle path was planned without accounting for soft tissue displacement, it was mitigated by assuming a large radius for the voxelized needle and estimating the target as the center of the LES. Nevertheless, it could also be extended with physics in the future, or real-time path replanning. To assist the investigator in inserting the biopsy needle, we opted to use a regulated photo stand. However, we observed that the setup had limitations in controlling the direction of the tool axis. Additionally, potential collisions with the phantom required adjustments to the setup, making the procedure less ergonomic and still time-consuming.

5. Conclusions

The study presents an approach for automating and supporting biopsy. A series of tests was conducted on a 3d printed brain phantom to assess its efficiency. The experiments confirmed good efficiency of the approach tools for planning and aiding biopsy in both software planning and hardware execution. Future studies will investigate the integration of a robotic manipulator to enhance procedural efficiency.

References

1. Abu-Dakka, F. J., Rubio, F., Valero, F., & Mata, V. (2013). Evolutionary indirect approach to solving trajectory planning problem for industrial robots operating in workspaces with obstacles. Eur. J. Mech. A Solids, 42, 210–218.
2. Badawi, A. M., & El-Mahdy, M. A. (2003). Path planning simulation for 3D ultrasound guided needle biopsy system. Proc. Midwest Symp. Circuits Syst., 1, 345–347.
3. Brunenberg, E. J. L., Vilanova, A., Visser-Vandewalle, V., Temel, Y., Ackermans, L., Platel, B., & Ter Haar Romeny, B. M. (2007). Automatic trajectory planning for deep brain stimulation: A feasibility study. In Med. Image Comput. Comput. Assist. Interv. – MICCAI, 4791, 584–592.
4. Christou, A. S., Amalou, A., Lee, H., Rivera, J., Li, R., Kassin, M. T., ... Wood, B. J. (2021). Image-guided robotics for standardized and automated biopsy and ablation. Semin. Interv. Radiol., 38(5), 565–575.
5. Ciszkiewicz, A., & Milewski, G. (2018). Path planning for minimally-invasive knee surgery using a hybrid optimization procedure. Comput. Methods Biomech. Biomed. Engin., 21(1), 47–54.
6. Ciszkiewicz, A., Lorkowski, J., & Milewski, G. (2022). Differential evolution and cost-maps for needle path planning in Baker's cyst aspiration. Acta Bioeng. Biomech., 24(4).
7. De Baere, T., Roux, C., Noel, G., Delpla, A., Deschamps, F., Varin, E., & Tselikas, L. (2022). Robotic assistance for percutaneous needle insertion in the kidney: Preclinical proof on a swine animal model. Eur. Radiol. Exp., 6(1), 13.
8. Drozd, D., & Ciszkiewicz, A. (2024). Fast segmentation of convex cyst-like structures in gelatin soft tissue phantoms under ultrasound imaging with artifacts and limited training samples. Adv. Sci. Technol. Res. J., 18(4), 89–96.
9. Fong, A. J., Stewart, C. L., Lafaro, K., LaRocca, C. J., Fong, Y., Femino, J. D., & Crawford, B. (2021). Robotic assistance for quick and accurate image-guided needle placement. Updates Surg., 73(3), 1197–1201.

10. Gao, F., & Han, L. (2012). Implementing the Nelder-Mead simplex algorithm with adaptive parameters. Comput. Optim. Appl., 51(1), 259–277.
11. Gromniak, M., Neidhardt, M., Heinemann, A., Püschel, K., & Schlaefer, A. (2020). Needle placement accuracy in CT-guided robotic post mortem biopsy. Curr. Dir. Biomed. Eng., 6, 20200031.
12. Hall, W. A., Liu, H., Martin, A. J., Maxwell, R. E., & Truwit, C. L. (2001). Brain biopsy sampling by using prospective stereotaxis and a trajectory guide. J. Neurosurg., 94(1), 67–71.
13. Leung, K. Y. E., & Bosch, J. G. (2007). Localized shape variations for classifying wall motion in echocardiograms. In Med. Image Comput. Comput. Assist. Interv. – MICCAI, 4791, 52–59.
14. Liang, K., Rogers, A. J., Light, E. D., Von Allmen, D., & Smith, S. W. (2010). Simulation of autonomous robotic multiple-core biopsy by 3D ultrasound guidance. Ultrason. Imaging, 32(2), 118–127.
15. Mahmoud, M. Z., Aslam, M., Alsaadi, M., Fagiri, M. A., & Alonazi, B. (2018). Evolution of robot-assisted ultrasound-guided breast biopsy systems. J. Radiat. Res. Appl. Sci., 11(1), 89–97.
16. Majak, M., Żuk, M., Świątek-Najwer, E., Popek, M., & Pietruski, P. (2021). Augmented reality visualization for aiding biopsy procedure according to computed tomography based virtual plan. Acta Bioeng. Biomech., 23(2).
17. Marcus, H. J., Vakharia, V. N., Sparks, R., Rodionov, R., Kitchen, N., McEvoy, A. W., ... Duncan, J. S. (2020). Computer-assisted versus manual planning for stereotactic brain biopsy: A retrospective comparative pilot study. Oper. Neurosurg., 18(4), 417–422.
18. Mason, D., scaramallion, mrbean-bremen, rhaxton, Suever, J., Orfanos, D. P., ... Sentner, T. (2024). Pydicom/pydicom: Pydicom 3.0.1 (version v3.0.1) [Software]. Zenodo.
19. Monfaredi, R., Concepcion-Gonzalez, A., Acosta Julbe, J., Fischer, E., Hernandez-Herrera, G., Cleary, K., & Oluigbo, C. (2024). Automatic path-planning techniques for minimally invasive stereotactic neurosurgical procedures—A systematic review. Sensors, 24(16), 5238.
20. Moustris, G. P., Hiridis, S. C., Deliparaschos, K. M., & Konstantinidis, K. M. (2011). Evolution of autonomous and semi-autonomous robotic surgical systems: A review of the literature. Int. J. Med. Robot., 7(4), 375–392.

21. Napalkova, L., Rozenblit, J. W., Hwang, G., Hamilton, A. J., & Suantak, L. (2014). An optimal motion planning method for computer-assisted surgical training. Appl. Soft Comput., 24, 889–899.
22. Navkar, N. V., Tsekos, N. V., Stafford, J. R., Weinberg, J. S., & Deng, Z. (2010). Visualization and planning of neurosurgical interventions with straight access. In Inf. Process. Comput. Assist. Interv., 6135, 1–11.
23. Pietruski, P., Majak, M., Świątek-Najwer, E., Żuk, M., Popek, M., Świecka, M., ... Mazurek, M. (2023). Replacing cutting guides with an augmented reality-based navigation system: A feasibility study in the maxillofacial region. Int. J. Med. Robot., 19(3), e2499.
24. Phee, L., Yuen, J., Xiao, D., Chan, C. F., Ho, H., Thng, C. H., ... Ng, W. S. (2006). Ultrasound guided robotic biopsy of the prostate. Int. J. Humanoid Robot., 3(4), 463–483.
25. Qureshi, A. H., & Ayaz, Y. (2015). Intelligent bidirectional rapidly-exploring random trees for optimal motion planning in complex cluttered environments. Robot. Auton. Syst., 68, 1–11.
26. Scharll, Y., Radojicic, N., Laimer, G., Schullian, P., & Bale, R. (2024). Puncture accuracy of robot-assisted CT-based punctures in interventional radiology: An ex vivo study. Diagnostics, 14(13), 1371.
27. Shi, M., Liu, H., Tao, G., & Fajardo, L. L. (1999). Stereofluoroscopic image-guided robotic biopsy system. In Proc. SPIE, 193–200.
28. Sparks, R., Vakharia, V., Rodionov, R., Vos, S. B., Diehl, B., Wehner, T., ... Ourselin, S. (2017). Anatomy-driven multiple trajectory planning (Admtp) of intracranial electrodes for epilepsy surgery. Int. J. Comput. Assist. Radiol. Surg., 12(8), 1245–1255.
29. Spenkelink, I. M., Heidkamp, J., Avital, Y., & Fütterer, J. J. (2023). Evaluation of the performance of robot assisted CT-guided percutaneous needle insertion: Comparison with freehand insertion in a phantom. Eur. J. Radiol., 162, 110753.
30. Starup-Hansen, J., Williams, S. C., Funnell, J. P., Hanrahan, J. G., Islam, S., Al-Mohammad, A., & Hill, C. S. (2023). Optimising trajectory planning for stereotactic brain tumour biopsy using artificial intelligence: A systematic review. Br. J. Neurosurg., 1–10.
31. Świątek-Najwer, E., Majak, M., Popek, M., & Żuk, M. (2022). “Image to patient” equal-resolution surface registration supported by a surface scanner: Analysis of algorithm efficiency for computer-aided surgery. Int. J. Comput. Assist. Radiol. Surg., 18(2), 319–328.

32. Tanaiutchawoot, N., Treepong, B., Wiratkapan, C., & Suthakorn, J. (2014). A path generation algorithm for biopsy needle insertion in a robotic breast biopsy navigation system. In Proc. IEEE ROBIO, 398–403.
33. Treepong, B., Tanaiutchawoot, N., Wiratkapun, C., & Suthakorn, J. (2014). On the design and development of a breast biopsy navigation system. Proc. IEEE BHI, 273–276.
34. Trope, M., Shamir, R. R., Joskowicz, L., Medress, Z., Rosenthal, G., Mayer, A., ... Shoshan, Y. (2015). The role of automatic computer-aided surgical trajectory planning in improving the expected safety of stereotactic neurosurgery. Int. J. Comput. Assist. Radiol. Surg., 10(7), 1127–1140.
35. Vaillant, M., Davatzikos, C., Taylor, R. H., & Bryan, R. N. (1997). A path-planning algorithm for image-guided neurosurgery. In CVRMed-MRCAS, 1205, 467–476.
36. Vakharia, V. N., & Duncan, J. S. (2020). Automation advances in stereoelectroencephalography planning. Neurosurg. Clin. N. Am., 31(3), 407–419.
37. Van Der Walt, S., Schönberger, J. L., Nunez-Iglesias, J., Boulogne, F., Warner, J. D., ... Yu, T. (2014). Scikit-image: Image processing in Python. PeerJ, 2, e453.
38. Virtanen, P., Gommers, R., Oliphant, T. E., Haberland, M., Reddy, T., ... Vázquez-Baeza, Y. (2020). SciPy 1.0: Fundamental algorithms for scientific computing in Python. Nat. Methods, 17(3), 261–272.
39. Xu, H., Lasso, A., Vikal, S., Guion, P., Krieger, A., ... Fichtinger, G. (2010). MRI-guided robotic prostate biopsy: A clinical accuracy validation. In Med. Image Comput. Comput. Assist. Interv., 13(Pt 3), 383–391.
40. Zhang, X., Lin, D., Pforsich, H., & Lin, V. W. (2020). Physician workforce in the United States of America: Forecasting nationwide shortages. Hum. Resour. Health, 18(1), 8.

Acknowledgement: We would like to express our deepest gratitude to Dr. Marcin Majak, an independent researcher collaborating with Wrocław University of Science and Technology, for his invaluable assistance in the development of the MentorEye software.

Author Contributions: Adam Ciszkiewicz 42,5%, A, B, D, E, Jakub Urban 5%, B, Grzegorz Ziółkowski 5%, B, Celina Pezowicz 5%, E, Ewelina Świątek-Najwer 42,5%, A, B, D, E. All authors have read and agreed to the published version of the manuscript.

Funding: This study applies and develops software created in frames of a project funded by National Centre of Research and Development in Poland, (grant number STRATEGMED1/233624/4/NCBR/ 2014, 'Development of Polish complementary system of molecular surgical navigation for tumor treatment').